

COMMUNICATION

[View Article Online](#)
[View Journal](#) | [View Issue](#)

Cite this: *Nanoscale Adv.*, 2024, **6**, 4352

Received 6th May 2024
Accepted 17th July 2024

DOI: 10.1039/d4na00378k

rsc.li/nanoscale-advances

Improving MPI and hyperthermia performance of superparamagnetic iron oxide nanoparticles through fractional factorial design of experiments[†]

Yanchen Li,^a Rui Zhang, Roman Barmin, Elena Rama,^a Max Schoenen, Franziska Schrank,^a Volkmar Schulz,^a Ioana Slabu, ^b Fabian Kiessling, Twan Lammers and Roger M. Pallares *

Superparamagnetic iron oxide nanoparticles (SPIONs) are widely used for biomedical applications, including magnetic particle imaging (MPI) and magnetic hyperthermia. The co-precipitation method is one of the most common synthetic routes to obtain SPIONs, since it is simple and does not require extreme conditions, such as high temperatures. Despite its prevalence, however, the co-precipitation synthesis presents some challenges, most notably the high batch-to-batch variability, as multiple factors can influence nanoparticle growth. In this study, we utilized a fractional factorial design of experiments to identify key factors influencing SPION growth, properties, and performance in MPI and magnetic hyperthermia, namely Fe^{3+} content, pH, temperature, stirring, and atmosphere. Notably, our study unveiled secondary interactions, particularly between temperature and Fe^{3+} content, as well as pH and Fe^{3+} content, for which simultaneous changes of both parameters promoted greater effects than the sum of each factor effect alone, emphasizing the impact of synergistic effects on SPION growth and performance. These findings provide a deeper understanding of the growth mechanism of SPIONs, reconcile discrepancies in the existing literature, and underscore the importance of characterizing secondary interactions to improve the performance of SPIONs for biomedical applications.

Introduction

Superparamagnetic iron oxide nanoparticles (SPIONs) are magnetic nanomaterials with unique physicochemical properties that are widely used for (pre)clinical diagnosis and therapy.^{1–5} For example, they display strong magnetic responses when exposed to an external magnetic field, which rapidly decrease when the magnetic field is removed. Their magnetic

properties are also exploited in magnetic particle imaging (MPI), an emerging imaging modality that relies on two opposing magnetic gradient fields to saturate the magnetization of SPIONs, except for those located in a field free region that are used as tracers.⁶ Among different (potential) applications, SPIONs have been used as MPI tracers for monitoring immune cell infiltration in pathological tissues during immunotherapy and for real-time imaging of perfusion.⁷ Furthermore, the heat released by SPIONs under the influence of alternating magnetic fields of sufficient strength and frequency can be used to locally ablate pathological tissues, such as tumors, in a therapeutic strategy known as magnetic hyperthermia.⁸ Beyond their magnetic properties, the surface of SPIONs can be easily functionalized with biocompatible ligands and targeting agents, endowing applications in molecular imaging and targeted therapeutics.^{9,10}

SPIONs are synthesized through different colloidal methods, including thermal decomposition,¹¹ co-precipitation,¹² sol-gel,¹³ and microemulsion.¹⁴ The co-precipitation method is frequently used, since it possesses several key advantages, including high yield, simplicity (e.g. no high temperatures are required), and production of water-soluble nanoparticles. However, it also presents limitations, such as batch-to-batch variability and poor control over SPION morphology and properties. This variability is likely caused by the effect of several factors (e.g. iron content, atmosphere, pH level, temperature, and stirring) that influence the growth of the SPIONs. Notably, previous works with SPIONs obtained through sonication methods and other nanoparticles, such as gold nanorods and gold nanostars, demonstrated that simultaneous changes of several factors during the synthesis of the nanoparticles have synergistic effects, which are greater than the sum of single factor changes.^{15–17} Understanding these multilevel factorial effects is crucial for nanoparticle growth and reducing synthesis variability.

Here, we investigated the primary and secondary interaction effects governing the synthesis and performance of SPIONs through a fractional factorial design of experiments (Scheme 1).

^aInstitute for Experimental Molecular Imaging, RWTH Aachen University Hospital, Aachen 52074, Germany. E-mail: rmoltopallar@ukaachen.de

^bInstitute for Applied Medical Engineering, RWTH Aachen University Hospital, Aachen 52074, Germany

[†] Electronic supplementary information (ESI) available: Materials and methods; table of fractional factorial design of experiments; TEM micrographs of synthesized SPIONs; size distributions of SPIONs; secondary interaction effects on SPION size, SNR measured by MPI, and SLP; magnetic hyperthermia curves of SPIONs. See DOI: <https://doi.org/10.1039/d4na00378k>



The synthesized SPIONs exhibited a nearly spherical shape. Both the size of SPIONs and the signal-to-noise ratio (SNR) in MPI increased with changes in temperature, Fe^{3+} content, and pH. However, the performance of SPIONs in magnetic hyperthermia was found to be less sensitive to the evaluated synthesis factors. Additionally, specific secondary interactions exerted greater effects than the sum of each individual factor effect. These findings offer new insights into the synthesis and performance of SPIONs, elucidating discrepancies in the literature concerning the impact of these specific factors.

Results and discussion

The synthesis of SPIONs *via* the co-precipitation method is commonly performed as follows:¹⁸ ferric chloride (8 mmol) and ferrous chloride (4 mmol) are mixed in deionized water, and the pH of the resulting solution is adjusted to 11. This mixture is left to react for 30 min at 25 °C under stirring in a nitrogen atmosphere. Subsequently, black iron oxide particles are formed, which are then magnetically separated, washed, and surface functionalized with trisodium citrate (0.25 g mL⁻¹) at 80 °C for 2 h. The resulting citrate-coated SPIONs are then magnetically separated, resuspended in deionized water, and filtered with a 0.2 µm filter to remove larger particulates. It is worth noting that SPIONs need to be functionalized (*e.g.* with dextran or PEG) to be stable in biological environments and be used either as therapeutic agents or imaging probes. In our current study, we have focused on their synthesis. Hence, the surface of the SPIONs is modified with citrate, which renders disperse nanoparticles in solution, but not in biological media. Our SPIONs would need to be further functionalized to be (pre) clinically used.

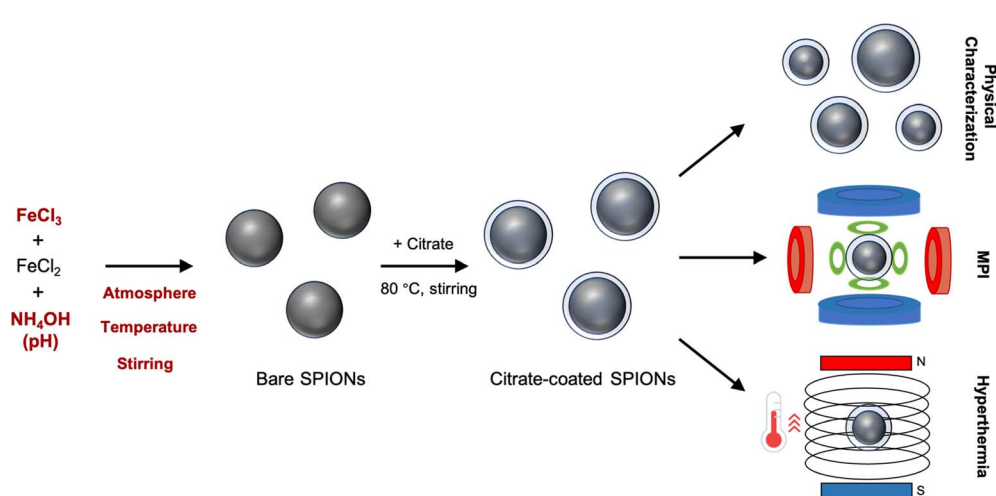
After performing the synthesis under these conditions, we obtained nanoparticles with spheroid-like shape and an average core diameter of 21.2 ± 3.8 nm, as observed by transmission electron microscopy (TEM) (Fig. 1a and b). The SPIONs

displayed superparamagnetic behavior as identified in the hysteretic $M(H)$ curves at 295 K, with an average saturation magnetization of 101.8 ± 0.7 A m² kg⁻¹, indicating strong magnetic responses to the external magnetic field (Fig. 1c). Furthermore, the synthesized SPIONs showed good imaging capabilities by generating intense signals in MPI (Fig. 1d). The SPIONs were also able to increase the temperature of the solution by 13.1 ± 0.2 °C when placed under the influence of an alternating magnetic field (frequency of 271 kHz and amplitude of 41 kA m⁻¹) in a custom-built hyperthermia setup (Fig. 1e).

In the current study, five key synthetic parameters were investigated through fractional factorial design of experiments (Table 1). These five factors were chosen based on previous reports, which identified them as parameters influencing the growth of SPIONs.^{18,19} Because the molar ratio of ferric chloride and ferrous chloride was kept constant at 2 : 1, only the variation of Fe^{3+} is shown in the table. Additionally, each factor was examined at two different levels. Hence, the resulting experimental design, known as 2_v^{5-1} , was comprised of 5 factors with 2 levels each, involving a total of 16 experiments (Table S1†). Notably, the 2_v^{5-1} design enables the identification of both primary and secondary interaction effects.^{20,21} The morphological characteristics of the SPIONs grown under each condition were characterized by TEM, and their performances as MPI tracers, and magnetic hyperthermia agents were also assessed.

Size of the SPIONs

The nanoparticles were synthesized under the different conditions reported in Table S1† in quadruplicate. Out of the sixteen conditions explored, four conditions (FFD 2, 6, 10 and 14 in Table S1†) with Fe^{3+} content of 40 mmol and pH of 9 did not yield SPIONs. This observation implies that SPIONs cannot be generated when the iron content is high and the pH is low simultaneously. In contrast, the rest of the conditions did allow the growth of SPIONs, which were characterized by TEM (Fig. S1 and S2†) and displayed inter-batch variabilities between 2.4 and



Scheme 1 Experimental design of the study. The five key factors (highlighted in red) governing the synthesis and performance of SPIONs were studied through a fractional factorial design of experiments. After the synthesis, the morphological characteristics of the SPIONs as well as their performance in MPI and magnetic hyperthermia were evaluated.



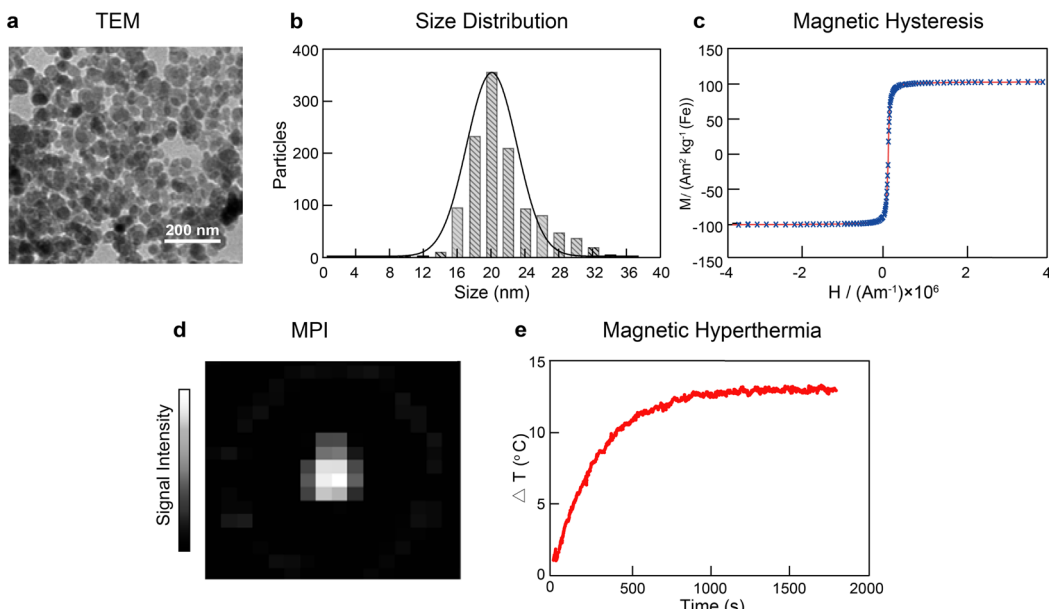


Fig. 1 SPIONs obtained with the standard co-precipitation method. (a) TEM micrographs of SPIONs. (b) Size distribution of SPIONs. (c) Field-dependent magnetization curve of SPIONs (2.8 mg mL^{-1}) at 295 K. (d) MPI intensity map of SPION solution ($0.8 \mu\text{L}, 20.1 \text{ mg mL}^{-1}$). (e) Time-temperature curves of SPIONs (1 mg mL^{-1}) under the influence of an alternating magnetic field at a frequency of 271 kHz and a field amplitude of 41 kA m^{-1} for 30 min.

6.8% (Table S2†). We initially characterized the effect of the five factors on the diameter of the SPIONs. Since *t*-tests tend to overestimate statistical significance when comparing large populations (in our case, between hundreds and thousands of nanoparticles per experimental group), we employed effect size (Cohen's *d*) to determine the strength of an effect when comparing two populations of sizes.²² Further details on the statistical analysis can be found in the materials and methods section.

The fractional factorial design showed that primary and secondary interaction effects of three factors determine the size of SPIONs (Fig. 2). These three key factors are temperature, Fe^{3+} content, and pH value (Cohen's *d* > 0.3). The statistical analysis of secondary interaction effects is displayed in Fig. S3.† It must be noted that the experimental data show a wide dispersion when presented as function of the primary interaction effects. This is because the data are displayed based on only one factor (e.g., low or high Fe^{3+} content), even though the values of the other four factors (e.g., temperature, pH, stirring, and atmosphere) may be different depending on the experimental

conditions set during the synthesis of each SPION batch (Table 1). Nevertheless, the 2^{5-1} fractional factorial design can discriminate primary and secondary interaction effects.^{20,21}

Our analysis demonstrated that Fe^{3+} content was the most significant factor, through both primary and several secondary interaction effects, in influencing the size of SPIONs (Cohen's *d* > 0.9). As Fe^{3+} content increased from low (8 mmol) to high (40 mmol), the diameter of the SPIONs increased by $4.1 \pm 0.2 \text{ nm}$. Additionally, secondary interaction effects of Fe^{3+} content could also increase the SPION diameter from $18.8 \pm 2.2 \text{ nm}$ up to $24.3 \pm 5.0 \text{ nm}$. The higher iron ion content endowed the growth of larger particles, likely because of the greater availability of iron in solution to be incorporated into the nanoparticles.

Moreover, an increase in solution pH also correlated with an augmented SPION diameter, influenced by both primary and secondary interaction effects (from 19.7 ± 2.0 up to $24.2 \pm 3.4 \text{ nm}$). Although the mechanism behind this observation is not fully understood, it is worth noting that increasing the pH from 9 to 11 promotes the formation of soluble iron hydroxide species (i.e. $\text{Fe}(\text{OH})_4^-$)²³ that may favor the formation of larger particles through different colloidal mechanisms, such as Ostwald ripening.^{24,25}

The third factor to affect SPION size was temperature. Increasing the temperature from 25°C to 80°C , led to an increase in particle size up to $26.1 \pm 3.3 \text{ nm}$, likely due to the faster nanoparticle growth kinetics at higher temperatures, which are known to induce larger particulates through different mechanisms, such coalescence and Ostwald ripening.^{24,26} Our quantitative results on the primary effects of temperature, Fe^{3+} content, and pH on SPION size align with qualitative observations previously published.²⁷

Table 1 Experimental conditions used for each factor, and their comparison to the standard protocol

Factors	Standard protocol	Low (-1)	High (+1)
A	Temperature	25°C	25°C
B	pH	11	9
C	Fe^{3+}	8 mmol	8 mmol
D	Atmosphere	N_2	Air
E	Stirring	100 rpm	0
			100 rpm



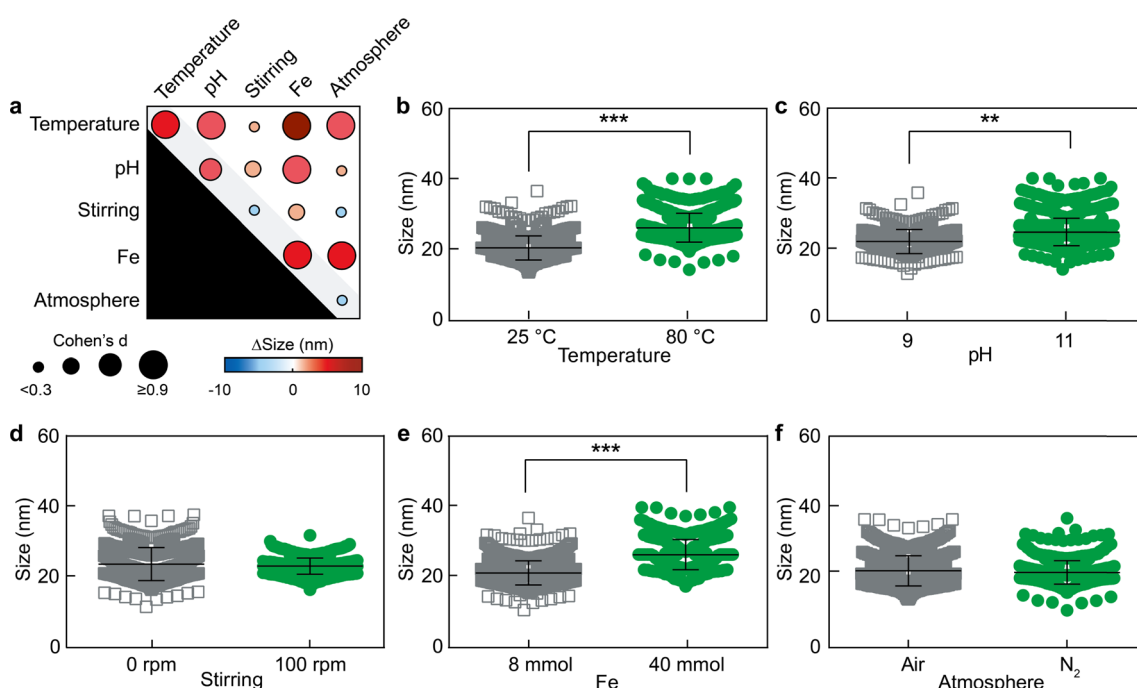


Fig. 2 Primary and secondary interaction effects on the SPION size. (a) Summary of the interaction effects, and primary interaction results of (b) temperature, (c) pH, (d) stirring, (e) Fe^{3+} content, and (f) atmosphere on SPION size (diameter). (**) and (***) indicate groups with large (Cohen's $d > 0.6$) and very large (Cohen's $d > 0.9$) effect sizes, respectively. Each data point represents the size of a measured particle. Four batches per condition were synthesized and more than 100 particles were measured per batch.

Notably, the most significant change in SPION diameter (increasing from 19.9 ± 3.8 nm to 28.3 ± 5.1 nm) was caused by the secondary interaction between temperature and Fe^{3+} content. This secondary interaction effect caused a greater size variation than the sum of each primary effect alone, demonstrating the importance of secondary interactions during the synthesis and growth of SPIONs.

SNR measured by MPI

MPI is an advanced imaging technique known for its high temporal and spatial resolution, allowing real-time 3D visualization of SPION distribution, providing valuable information on their localization and concentration.²⁸⁻³¹ SNR is a critical metric in MPI, as a higher SNR enhances the quality and reliability of the images by minimizing unwanted noise and maximizing the clarity of the signal.³²

Therefore, the primary and secondary effects of the five factors on the SNR of SPIONs during MPI measurements were characterized. To compare the MPI performance of the various samples, SNR values were normalized to the iron concentration of each sample. Both primary and secondary interaction effects, including variations in Fe^{3+} content, pH, and temperature, were found to statistically influence the magnitude of SNR measured by MPI (Fig. 3). These observations were consistent with the results obtained for size variations in Fig. 2. For example, Fe^{3+} content was the strongest factor affecting SPION diameter, increasing nanoparticle size through primary and secondary interaction effects. Consistently, as Fe^{3+} content increased from low (8 mmol) to high (40 mmol) values, the SNR strength escalated from $10.6 \pm 1.7 \times 10^3$ to $22.1 \pm 1.1 \times 10^3$.

Moreover, varying the pH from 9 to 11 and the temperature from 25 °C to 80 °C increased the SNR by $2.9 \pm 2.3 \times 10^3$ and $8.7 \pm 1.6 \times 10^3$, respectively. The statistical analysis of secondary interaction effects on SNR is reported in Fig. S4.† Notably, two secondary interactions, namely pH-stirring and Fe-stirring, caused the most pronounced effects on the SNR as measured by MPI, increasing the SNR up to $26.8 \pm 1.4 \times 10^3$ and $24.8 \pm 1.3 \times 10^3$, respectively. This is puzzling because variations of stirring alone have almost no discernible impact on SNR, and the primary effects of pH or iron content are notably less pronounced than those observed in the context of pH-stirring or Fe-stirring. These results further highlighted the importance of secondary effects, which can be larger than the sum of the effects of each factor alone.

Temperature changes observed during magnetic hyperthermia

When SPIONs are placed in an alternating magnetic field on the order of a few hundred kHz, their magnetic moments continuously reorient following the field direction, which causes the local release of heat due to relaxation losses.³³ This principle has been extensively explored in preclinical settings for local thermal ablation of pathological tissue (magnetic hyperthermia) in treatments against different types of tumors, and is currently being explored in a clinical trial against advanced pancreatic cancer.³⁴

The evaluation of heating performance involves the measurement of the specific loss power (SLP), which represents the thermal loss per unit mass under the influence of an applied

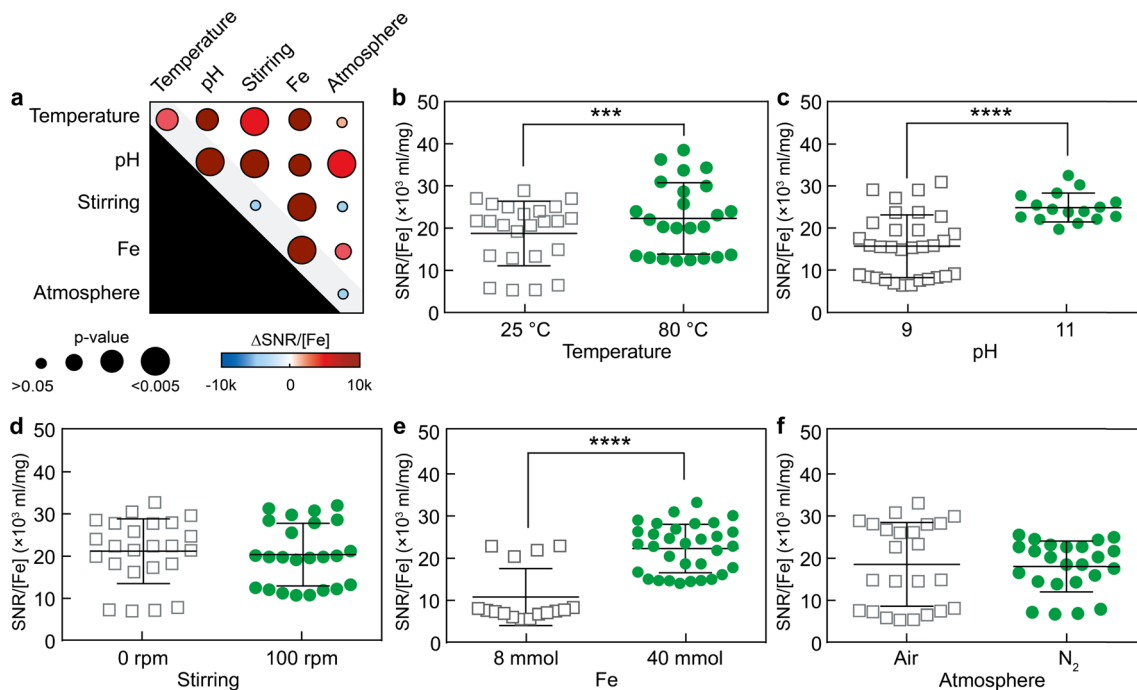


Fig. 3 Primary and secondary interaction effects on the SNR as measured by MPI. (a) Summary of the interaction effects, and primary interaction results of (b) temperature, (c) pH, (d) stirring, (e) Fe^{3+} content, and (f) atmosphere on SNR of SPIONs as measured by MPI. (*** and ****) indicate groups that are significantly different with $p < 0.001$, and $p < 0.0001$, respectively (independent two-sample t-test). Each data point represents the SNR of a batch solution. Four batches were tested per condition.

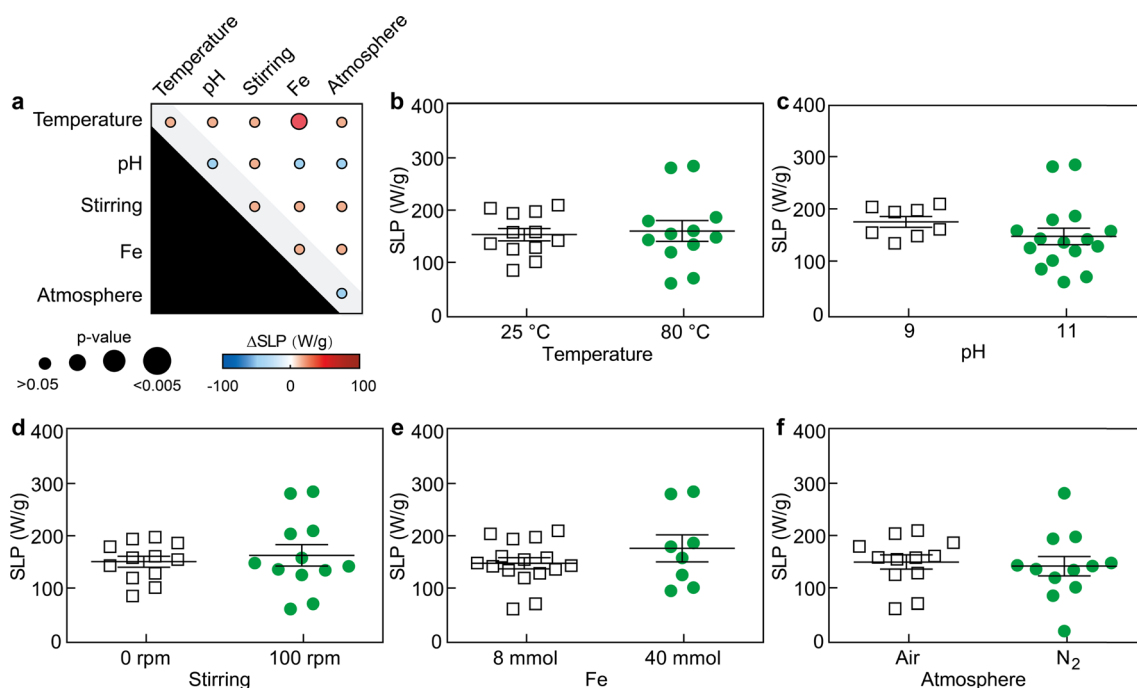


Fig. 4 Primary and secondary interaction effects on the SLP. (a) Summary of the interaction effects, and primary interaction results of (b) temperature, (c) pH, (d) stirring, (e) Fe^{3+} content, and (f) atmosphere on SPION performance in magnetic hyperthermia. Each data point represents the SLP of a batch solution. Two batches were tested per condition.

magnetic field.^{35,36} To assess SLP values, we conducted temperature–time curve measurements for each sample at a concentration of 1 mg mL^{−1} under the influence of an alternating magnetic field (frequency of 271 kHz and amplitude of 41 kA m^{−1}), as depicted in Fig. S5.† Further details on the SLP calculations can be found in the Materials and methods section.

By characterizing the primary and secondary effects of the five factors on the magnetic hyperthermia performance of the resulting SPIONs, we observed that SLP values were barely statistically affected by either primary or secondary interaction effects (Fig. 4 and S6†). As previously discussed, the data show large variability within groups when displayed as function of the primary interaction effects, since the results are presented based on one factor (e.g., low or high pH) independently of the values of the other four factors (e.g., temperature, Fe³⁺ content, stirring, and atmosphere) set during the experiment. Only the Fe³⁺ content – temperature effects did statistically alter (increased) the SLP value ($p < 0.05$). These results seem to suggest the performance of SPIONs for magnetic hyperthermia is less sensitive to the synthetic factors evaluated, and perhaps, stronger variations of those factors would be necessary to cause changes in their SLP and further improve their performance.

Conclusion

In summary, we employed a fractional factorial design of experiments to unravel the key factors influencing the co-precipitation synthesis of SPIONs and their performance in MPI, and magnetic hyperthermia. Fe³⁺ content, pH, and temperature, either individually or particularly in combination with other factors, were found to impact the size of SPIONs the most. Notably, changes in stirring alone had minimal effects but exhibited a significant impact on the SNR of MPI when combined with other factors. Magnetic hyperthermia was the application less affected by changes in the five factors, and only simultaneous variations of temperature and iron content increased the SLP of the particles. These findings underscore the intricate nature of the factors governing the growth of SPIONs and emphasize the importance of characterizing secondary interaction effects for tailoring nanoparticles with desired properties to specific applications.

Data availability

The data supporting this article have been included as part of the ESI.†

Author contributions

Y. L. and R. M. P. designed the research; Y. L. carried out the synthesis and characterization of the nanoparticles; R. Z., R. B. and E. R. assisted in the experiments; M. S. and I. S. performed the magnetic hyperthermia tests; F. S. carried out the MPI experiments; V. S., F. K., T. L. and R. M. P. provided scientific guidance; Y. L. wrote the first manuscript draft; all authors reviewed the manuscript.

Conflicts of interest

The authors have no relevant affiliations or financial involvement with any organization or entity with a financial interest in or financial conflict with the subject matter or materials discussed in the manuscript.

Acknowledgements

This work is funded by the Federal Ministry of Education and Research (BMBF), by the Ministry of Culture and Science of the German State of North Rhine-Westphalia under the Excellence Strategy of the Federal Government and the Länder through the RWTH Junior Principal Investigator (JPI) fellowship scheme, by the European Research Council (ERC; 864121, and 101076174), and by the German Research Foundation (DFG; GRK2375 (331065168), PAK 961 (403039938), FOR5011 (CRU 5011/445703531), 467959793, and SFB1066).

References

- 1 F. Cheng, Characterization of Aqueous Dispersions of Fe₃O₄ Nanoparticles and Their Biomedical Applications, *Biomaterials*, 2005, **26**(7), 729–738, DOI: [10.1016/j.biomaterials.2004.03.016](https://doi.org/10.1016/j.biomaterials.2004.03.016).
- 2 R. Jin, B. Lin, D. Li and H. Ai, Superparamagnetic Iron Oxide Nanoparticles for MR Imaging and Therapy: Design Considerations and Clinical Applications, *Curr. Opin. Pharmacol.*, 2014, **18**, 18–27, DOI: [10.1016/j.coph.2014.08.002](https://doi.org/10.1016/j.coph.2014.08.002).
- 3 N. Lee and T. Hyeon, Designed Synthesis of Uniformly Sized Iron Oxide Nanoparticles for Efficient Magnetic Resonance Imaging Contrast Agents, *Chem. Soc. Rev.*, 2012, **41**(7), 2575–2589, DOI: [10.1039/C1CS15248C](https://doi.org/10.1039/C1CS15248C).
- 4 J. McCarthy and R. Weissleder, Multifunctional Magnetic Nanoparticles for Targeted Imaging and Therapy, *Adv. Drug Delivery Rev.*, 2008, **60**(11), 1241–1251, DOI: [10.1016/j.addr.2008.03.014](https://doi.org/10.1016/j.addr.2008.03.014).
- 5 H. Xu, L. Cheng, C. Wang, X. Ma, Y. Li and Z. Liu, Polymer Encapsulated Upconversion Nanoparticle/Iron Oxide Nanocomposites for Multimodal Imaging and Magnetic Targeted Drug Delivery, *Biomaterials*, 2011, **32**(35), 9364–9373, DOI: [10.1016/j.biomaterials.2011.08.053](https://doi.org/10.1016/j.biomaterials.2011.08.053).
- 6 O. C. Sehl, J. J. Gevaert, K. P. Melo, N. N. Knier and P. J. Foster, A Perspective on Cell Tracking with Magnetic Particle Imaging, *Tomography*, 2020, **6**(4), 315–324, DOI: [10.18383/j.tom.2020.00043](https://doi.org/10.18383/j.tom.2020.00043).
- 7 R. M. Pallares, F. M. Mottaghy, V. Schulz, F. Kiessling and T. Lammers, Nanoparticle Diagnostics and Theranostics in the Clinic, *J. Nucl. Med.*, 2022, **63**(12), 1802–1808, DOI: [10.2967/jnumed.122.263895](https://doi.org/10.2967/jnumed.122.263895).
- 8 C. Blanco-Andujar, A. Walter, G. Cotin, C. Bordeianu, D. Mertz, D. Felder-Flesch and S. Begin-Colin, Design of Iron Oxide-Based Nanoparticles for MRI and Magnetic Hyperthermia, *Nanomedicine*, 2016, **11**(14), 1889–1910, DOI: [10.2217/nmm-2016-5001](https://doi.org/10.2217/nmm-2016-5001).

9 M. Mahmoudi, S. Sant, B. Wang, S. Laurent and T. Sen, Superparamagnetic Iron Oxide Nanoparticles (SPIONs): Development, Surface Modification and Applications in Chemotherapy, *Adv. Drug Delivery Rev.*, 2011, **63**(1–2), 24–46, DOI: [10.1016/j.addr.2010.05.006](https://doi.org/10.1016/j.addr.2010.05.006).

10 N. Schleich, F. Danhier and V. Préat, Iron Oxide-Loaded Nanotheranostics: Major Obstacles to in Vivo Studies and Clinical Translation, *J. Controlled Release*, 2015, **198**, 35–54, DOI: [10.1016/j.jconrel.2014.11.024](https://doi.org/10.1016/j.jconrel.2014.11.024).

11 J. Park, K. An, Y. Hwang, J.-G. Park, H.-J. Noh, J.-Y. Kim, J.-H. Park, N.-M. Hwang and T. Hyeon, Ultra-Large-Scale Syntheses of Monodisperse Nanocrystals, *Nat. Mater.*, 2004, **3**(12), 891–895, DOI: [10.1038/nmat1251](https://doi.org/10.1038/nmat1251).

12 W. Wu, Z. Wu, T. Yu, C. Jiang and W.-S. Kim, Recent Progress on Magnetic Iron Oxide Nanoparticles: Synthesis, Surface Functional Strategies and Biomedical Applications, *Sci. Technol. Adv. Mater.*, 2015, **16**(2), 023501, DOI: [10.1088/1468-6996/16/2/023501](https://doi.org/10.1088/1468-6996/16/2/023501).

13 O. M. Lemine, K. Omri, M. Iglesias, V. Velasco, P. Crespo, P. De La Presa, L. El Mir, H. Bouzid, A. Yousif and A. Al-Hajry, γ -Fe₂O₃ by Sol-Gel with Large Nanoparticles Size for Magnetic Hyperthermia Application, *J. Alloys Compd.*, 2014, **607**, 125–131, DOI: [10.1016/j.jallcom.2014.04.002](https://doi.org/10.1016/j.jallcom.2014.04.002).

14 C. Okoli, M. Sanchez-Dominguez, M. Boutonnet, S. Järås, C. Civera, C. Solans and G. R. Kuttuva, Comparison and Functionalization Study of Microemulsion-Prepared Magnetic Iron Oxide Nanoparticles, *Langmuir*, 2012, **28**(22), 8479–8485, DOI: [10.1021/la300599q](https://doi.org/10.1021/la300599q).

15 J. C. Echeverría, P. Moriones, J. J. Garrido, M. D. Ugarte, L. Cervera, E. Garaio, C. Gómez-Polo and J. I. Pérez-Landazábal, Steering the Synthesis of Fe₃O₄ Nanoparticles under Sonication by Using a Fractional Factorial Design, *Mater. Chem. Phys.*, 2021, **270**, 124760, DOI: [10.1016/j.matchemphys.2021.124760](https://doi.org/10.1016/j.matchemphys.2021.124760).

16 N. D. Burrows, S. Harvey, F. A. Idesis and C. J. Murphy, Understanding the Seed-Mediated Growth of Gold Nanorods through a Fractional Factorial Design of Experiments, *Langmuir*, 2017, **33**(8), 1891–1907, DOI: [10.1021/acs.langmuir.6b03606](https://doi.org/10.1021/acs.langmuir.6b03606).

17 R. Zhang, F. Kiessling, T. Lammers and R. M. Pallares, Unraveling the Seedless Growth of Gold Nanostars through Fractional Factorial Design, *J. Phys. Chem. C*, 2022, **126**(43), 18580–18585, DOI: [10.1021/acs.jpcc.2c06396](https://doi.org/10.1021/acs.jpcc.2c06396).

18 S. M. Dadfar, D. Camozzi, M. Darguzyte, K. Roemhild, P. Varvarà, J. Metselaar, S. Banala, M. Straub, N. Güvener, U. Engelmann, I. Slabu, M. Buhl, J. Van Leusen, P. Kögerler, B. Hermanns-Sachweh, V. Schulz, F. Kiessling and T. Lammers, Size-Isolation of Superparamagnetic Iron Oxide Nanoparticles Improves MRI, MPI and Hyperthermia Performance, *J. Nanobiotechnol.*, 2020, **18**(1), 22, DOI: [10.1186/s12951-020-0580-1](https://doi.org/10.1186/s12951-020-0580-1).

19 S. M. Dadfar, K. Roemhild, N. I. Drude, S. Von Stillfried, R. Knüchel, F. Kiessling and T. Lammers, Iron Oxide Nanoparticles: Diagnostic, Therapeutic and Theranostic Applications, *Adv. Drug Delivery Rev.*, 2019, **138**, 302–325, DOI: [10.1016/j.addr.2019.01.005](https://doi.org/10.1016/j.addr.2019.01.005).

20 J. G. Voelkel, The Efficiencies of Fractional Factorial Designs, *Technometrics*, 2005, **47**(4), 488–494, DOI: [10.1198/04017005000000274](https://doi.org/10.1198/04017005000000274).

21 R. F. Gunst and R. L. Mason, Fractional Factorial Design, *WIREs Comput. Stat.*, 2009, **1**(2), 234–244, DOI: [10.1002/wics.27](https://doi.org/10.1002/wics.27).

22 J.-C. Goulet-Pelletier and D. Cousineau, A Review of Effect Sizes and Their Confidence Intervals, Part I: The Cohen's d Family, *The Quantitative Methods for Psychology*, 2018, **14**(4), 242–265, DOI: [10.20982/tqmp.14.4.p242](https://doi.org/10.20982/tqmp.14.4.p242).

23 F. Millero, Speciation of Metals in Natural Waters, *Geochem. Trans.*, 2001, **2**(1), 57, DOI: [10.1186/1467-4866-2-57](https://doi.org/10.1186/1467-4866-2-57).

24 J. A. A. Abdullah, M. Jiménez-Rosado, A. Guerrero and A. Romero, Effect of Calcination Temperature and Time on the Synthesis of Iron Oxide Nanoparticles: Green vs. Chemical Method, *Materials*, 2023, **16**(5), 1798, DOI: [10.3390/ma16051798](https://doi.org/10.3390/ma16051798).

25 G. Madras and B. J. McCoy, Ostwald Ripening with Size-Dependent Rates: Similarity and Power-Law Solutions, *J. Chem. Phys.*, 2002, **117**(17), 8042–8049, DOI: [10.1063/1.1510769](https://doi.org/10.1063/1.1510769).

26 A. H. M. Yusoff, M. N. Salimi and M. F. Jamlos, Critical Parametric Study on Final Size of Magnetite Nanoparticles, *IOP Conf. Ser.: Mater. Sci. Eng.*, 2018, **318**, 012020, DOI: [10.1088/1757-899X/318/1/012020](https://doi.org/10.1088/1757-899X/318/1/012020).

27 S. Vikram, M. Dhakshnamoorthy, R. Vasanthakumari, A. R. Rajamani, M. Rangarajan and T. Tsuzuki, Tuning the Magnetic Properties of Iron Oxide Nanoparticles by a Room-Temperature Air-Atmosphere (RTAA) Co-Precipitation Method, *J. Nanosci. Nanotechnol.*, 2015, **15**(5), 3870–3878, DOI: [10.1166/jnn.2015.9544](https://doi.org/10.1166/jnn.2015.9544).

28 M. H. Pablico-Lansigan, S. F. Situ and A. C. S. Samia, Magnetic Particle Imaging: Advancements and Perspectives for Real-Time in Vivo Monitoring and Image-Guided Therapy, *Nanoscale*, 2013, **5**(10), 4040, DOI: [10.1039/c3nr00544e](https://doi.org/10.1039/c3nr00544e).

29 Y. Lu, A. Rivera-Rodriguez, Z. W. Tay, D. Hensley, K. L. B. Fung, C. Colson, C. Saayujya, Q. Huynh, L. Kabuli, B. Fellows, P. Chandrasekharan, C. Rinaldi and S. Conolly, Combining Magnetic Particle Imaging and Magnetic Fluid Hyperthermia for Localized and Image-Guided Treatment, *Int. J. Hyperthermia*, 2020, **37**(3), 141–154, DOI: [10.1080/02656736.2020.1853252](https://doi.org/10.1080/02656736.2020.1853252).

30 N. Talebloo, M. Gudi, N. Robertson and P. Wang, Magnetic Particle Imaging: Current Applications in Biomedical Research, *Magn. Reson. Imaging*, 2020, **51**(6), 1659–1668, DOI: [10.1002/jmri.26875](https://doi.org/10.1002/jmri.26875).

31 J. Weizenecker, B. Gleich, J. Rahmer, H. Dahnke and J. Borgert, Three-Dimensional Real-Time *in Vivo* Magnetic Particle Imaging, *Phys. Med. Biol.*, 2009, **54**(5), L1–L10, DOI: [10.1088/0031-9155/54/5/L01](https://doi.org/10.1088/0031-9155/54/5/L01).

32 P. W. Goodwill and S. M. Conolly, The X-Space Formulation of the Magnetic Particle Imaging Process: 1-D Signal, Resolution, Bandwidth, SNR, SAR, and Magnetostimulation, *IEEE Trans. Med. Imaging*, 2010, **29**(11), 1851–1859, DOI: [10.1109/TMI.2010.2052284](https://doi.org/10.1109/TMI.2010.2052284).

33 S. Laurent, S. Dutz, U. O. Häfeli and M. Mahmoudi, Magnetic Fluid Hyperthermia: Focus on Superparamagnetic Iron Oxide Nanoparticles, *Adv. Colloid Interface Sci.*, 2011, **166**(1–2), 8–23, DOI: [10.1016/j.cis.2011.04.003](https://doi.org/10.1016/j.cis.2011.04.003).

34 I. Rubia-Rodríguez, A. Santana-Otero, S. Spassov, E. Tombácz, C. Johansson, P. De La Presa, F. J. Teran, M. D. P. Morales, S. Veintemillas-Verdaguer, N. T. K. Thanh, M. O. Besenhard, C. Wilhelm, F. Gazeau, Q. Harmer, E. Mayes, B. B. Manshian, S. J. Soenen, Y. Gu, Á. Millán, E. K. Efthimiadou, J. Gaudet, P. Goodwill, J. Mansfield, U. Steinhoff, J. Wells, F. Wiekhorst and D. Ortega, Whither Magnetic Hyperthermia? A Tentative Roadmap, *Materials*, 2021, **14**(4), 706, DOI: [10.3390/ma14040706](https://doi.org/10.3390/ma14040706).

35 A. Makridis, S. Curto, G. C. Van Rhoon, T. Samaras and M. Angelakeris, A Standardisation Protocol for Accurate Evaluation of Specific Loss Power in Magnetic Hyperthermia, *J. Phys. D: Appl. Phys.*, 2019, **52**(25), 255001, DOI: [10.1088/1361-6463/ab140c](https://doi.org/10.1088/1361-6463/ab140c).

36 B. Kozissnik, A. C. Bohorquez, J. Dobson and C. Rinaldi, Magnetic Fluid Hyperthermia: Advances, Challenges, and Opportunity, *Int. J. Hyperthermia*, 2013, **29**(8), 706–714, DOI: [10.3109/02656736.2013.837200](https://doi.org/10.3109/02656736.2013.837200).

